Holocene climates of the Iberian Peninsula: pollen-based reconstructions of changes in the west-east gradient of temperature and moisture

Mengmeng Liu[1,*], Yicheng Shen[2], Penelope González-Sampériz[3], Graciela Gil-Romera[3], Cajo J. F. ter Braak[4], Iain Colin Prentice[1], Sandy P. Harrison[2]

1: Department of Life Sciences, Imperial College London, Silwood Park Campus, Buckhurst Road, Ascot SL5 7PY, UK

2: Geography & Environmental Science, Reading University, Whiteknights, Reading, RG6 6AH, UK

3: Instituto Pirenaico de Ecología-CSIC, Avda. Montañana 1005, 50059, Zaragoza, Spain

4: Biometris (Applied Mathematics and Applied Statistics Centre), Wageningen University & Research, 6708 PB Wageningen, The Netherlands

*: Corresponding author: Mengmeng Liu (m.liu18@imperial.ac.uk)

Ms for: *Climate of the Past*

Abstract

The Iberian Peninsula is characterised by a steep west-east moisture gradient today, reflecting the dominance of maritime influences along the Atlantic coast and more Mediterranean-type climate further east. Holocene pollen records from the Peninsula suggest that this gradient was less steep during the mid-Holocene, possibly reflecting the impact of orbital changes on circulation and thus regional patterns in climate. Here we use 7214 pollen samples from 117 sites covering part or all of the last 12,000 years to reconstruct changes in seasonal temperature and in moisture across the Iberian Peninsula quantitatively. We show that there is an increasing trend in winter temperature at a regional scale, consistent with known changes in winter insolation. However, summer temperatures do not show the decreasing trend through the Holocene that would be expected if they were a direct response to insolation forcing. We show that summer temperature is strongly correlated with plant-available moisture (α), as measured by the ratio of actual evapotranspiration to equilibrium evapotranspiration, which declines through the Holocene. The reconstructions also confirm that the west-east gradient in moisture was considerably less steep than today during the mid-Holocene, indicating that atmospheric circulation changes (possibly driven by orbital changes) have been important determinants of the Holocene climate of the region.

1. Introduction

The Iberian Peninsula is characterised by a steep west-east gradient in temperature and moisture today, reflecting the dominance of maritime influences along the Atlantic coast and more Mediterranean-type climate further east. Projections of future climate change suggest that the region will become both warmer and drier, but nevertheless show that this west-east differentiation is maintained (Andrade et al., 2021a). The changes in temperature are projected to be larger and the occurrence of extreme temperature episodes more frequent in the south-central and eastern parts of Iberia than in Atlantic coastal areas (Carvalho et al., 2021). Similar gradients are seen in future projections of precipitation change, with largest reductions in precipitation in the south-central region (Andrade et al., 2021b). However, the stability of these west-east gradients during the Holocene has been questioned. In particular, the west-east gradient in moisture appears to have been less pronounced during the middle Holocene (8-4 ka) when cooler summers and wetter conditions in the Atlantic zone (e.g. Martínez-Cortizas et al., 2009; Mauri et al., 2015) coincided with the maximum development of mesophytic vegetation further east and south (Aranbarri et al., 2014, 2015; Carrión et al., 2010, 2009; González-Sampériz et al., 2017).

However, much of the evidence for Holocene climates of the Iberian Peninsula is based on qualitative interpretations of vegetation changes, generally interpreted as reflecting changes in moisture availability (Morellón et al., 2018). These records are extensive and they seem to indicate fairly complex spatial patterns of change. Kaufman et al. (2020) provides quantitative reconstructions of summer and winter temperature in their compilation of Holocene climate information, but there are only 5 terrestrial sites from the Iberian Peninsula. Iberia was also included in the quantitative pollen-based reconstructions of European climate through the Holocene (Mauri et al., 2015). However, the geographical distribution of sites included is uneven and a large fraction of the records were from the Pyrenees and the Cantabrian mountains, with additional clustering of sites in coastal regions. Thus, the inferred patterns of climate over most of the central part of the Peninsula are therefore largely extrapolated. Tarroso et al. (2016) has provided reconstructions of summer and winter temperature and mean annual precipitation since the Last Glacial Maximum for the Iberian Peninsula, by using modern species distribution data to develop climate probability distribution functions (PDFs) and applying these to 31 fossil records. However, although they identified trends in precipitation during the Holocene, the temperature reconstructions do not seem to be reliable since they show no changes through time (9 ~ 3 ka), either for the Iberian Peninsula as a whole or for individual sub-regions, in contra-distinction to the other reconstructions. The current state of uncertainty about Holocene climate changes in Iberia is further exacerbated because quantitative reconstructions of summer temperature made at individual sites using chironomid data (Muñoz Sobrino et al., 2013; Tarrats et al., 2018) are not consistent with reconstructed summer temperatures based on pollen for the same sites.

Here we re-examine the trends in summer and winter temperature and plant-available moisture through the Holocene across Iberia, using a new and relatively comprehensive compilation of pollen data (Shen et al., 2021) with age models based on the latest radiocarbon calibration curve (IntCal20: Reimer et al., 2020). We explicitly test whether there are significant differences in the west-east gradient of moisture and temperature through time. We then analyse the relationships between the changes in the three climate variables and how trends in these variables are related to external climate forcing. These analyses allow us to confirm that the west-east gradient in moisture was less steep during the mid-Holocene and indicate the importance of changes in atmospheric circulation in explaining observed patterns of climate change across the region.

2. Methods

Multiple techniques have been developed to make quantitative climate reconstructions from pollen (see reviews in Bartlein et al., 2011; Chevalier et al., 2020; Salonen et al., 2011). Modern analogue techniques (MAT: Overpeck et al., 1985) tend to produce rapid shifts in reconstructed values corresponding to changes in the selection of the specific analogue samples, although this tendency is less marked in the conceptually analogous response surface technique (Bartlein et al., 1986). Regression-based techniques, including weighted averaging methods such as Weighted Average Partial Least-Squares (WAPLS: ter Braak and Juggins, 1993), do not produce step-changes in the reconstructions but suffer from the tendency to compress the reconstructions towards the central part of the sampled climate range. However, this tendency can be substantially reduced by accounting for the sampling frequency (fx) and the climate tolerance of the pollen taxa present in the training data set (fxTWA-PLS: Liu et al., 2020). Bayesian approaches have also been applied to derive climate reconstructions from pollen assemblages (Peyron et al., 1998). However, comparison of fxTWA-PLS with the Bayesian model BUMPER (Holden et al., 2017), shows that fxTWA-PLS performs better in capturing the climate of the modern training data set from Europe (Liu et al., 2020).

Although fxTWA-PLS has clear advantages over other quantitative reconstructions techniques, there is still a slight tendency towards compression. We have therefore made a further modification to the approach as described in Liu et al. (2020). In the original version of fxTWA-PLS, the fx correction is applied as a weight with the form of $1/fx^2$ in the regression (step 7 in Table 1 in Liu et al., 2020). Here (see Appendix A) we make a further modification of fxTWA-PLS by (a) applying the fx correction separately in both the taxon calculation and the regression (step 2 and 7 in Table 1 in Liu et al., 2020) as a weight with the form of 1/fx and (b) applying P-splines smoothing (Eilers and Marx, 2021) in order to reduce the dependence of the fx estimation on bin width. The modified version further reduces the biases at the extremes of the sampled climate range. We used this modified version of fxTWA-PLS to reconstruct three climate variables: mean temperature of the coldest month (MTCO), mean temperature of the warmest month (MTWA) and plant-available moisture represented by α, an estimate of the ratio of actual evapotranspiration to equilibrium evapotranspiration. The individual and joint effects of MTCO, MTWA and α were tested explicitly using canonical correspondence analysis (CCA).

The modern pollen training dataset was derived from the SPECIAL Modern Pollen Data Set (SMPDS: Harrison, 2019). The SMPDS consists of relative abundance records from 6458 terrestrial sites from Europe, northern Africa, the Middle East and northern Eurasia (SI Figure S1) assembled from multiple different published sources. The pollen records were taxonomically standardized, and filtered (as recommended by Chevalier et al., 2020) to remove obligate aquatics, insectivorous species, introduced species, and taxa that only occur in cultivation. Taxa (mainly herbaceous) with only sporadic occurrences were amalgamated to higher taxonomic levels (genus, sub-family or family) after ensuring consistency with their distribution in climate space. As a result of these amalgamations, the SMPDS contains data on 247 pollen taxa. For our analysis, we use the 195 taxa that occur at more than 10 sites.

Modern climate data at each of the sites in the training data set were obtained from Harrison (2019). This data set contains climate reconstructions of MTCO, growing degree days above a baseline of 0° C (GDD_0) and a moisture index (MI), defined as the ratio of annual precipitation to annual potential evapotranspiration. The climate at each site was obtained using geographically-weighted regression of the CRU CL v2.0 gridded dataset of modern (1961-1990) surface climate at 10 arc minute resolution (New et al., 2002) in order to correct for elevation differences between each pollen site and the corresponding grid cell. The geographically-weighted regression used a fixed bandwidth kernel of 1.06 ° (~140km) to optimize model diagnostics and reduce spatial clustering of residuals relative to other bandwidths. The climate of each pollen site was then estimated based on its longitude, latitude, and elevation. MTCO and GDD_0 was taken directly from the GWR regression and MI was calculated for each pollen site using code modified from SPLASH v1.0 (Davis et al., 2017) based on daily values of precipitation, temperature and sunshine hours again obtained using a mean-conserving interpolation of the monthly values of each. For this application, we used MTCO directly from the data set but calculated MTWA from MTCO and GDD_0, based on the relationship between MTCO, MTWA and GDD_0 given by Appendix 2 of Wei et al. (2021). We derived α from MI following Liu et al. (2020). The modern training data set provides records spanning a range of MTCO from – 42.4 °C to 14.8 °C, of MTWA from 4.2 °C to 33.5 °C, and of α from 0.04 to 1.25 (Figure 1, SI Fig. S1).

The fossil pollen data from the Iberian Peninsula were compiled by Shen et al. (2021) and the data set (Harrison et al., 2022) was obtained from https://doi.org/10.17864/1947.000369. The taxonomy used by Shen et al. (2021) is consistent with that employed in the SMPDS. Shen et al. (2021) provides consistent age models for all the records based on the IntCal20 calibration curve (Reimer et al., 2020) and the BACON Bayesian age-modelling tool (Blaauw et al., 2021; Blaauw and Christeny, 2011) using the supervised modelling approach implemented in the `ageR` package (Villegas-Diaz et al, 2021). We excluded individual pollen samples with large uncertainties (standard error larger than 100 years) on the attributed in the new age model. As a result, the climate reconstructions are based on a fossil data set of 7384 pollen samples from 117 records covering part or all of the last 12,000 years (Figure 2), with 42 individual records provided by the original authors, 73 records obtained from the European Pollen Database (EPD, www.europeanpollendatabase.net) and 2 records from PANGAEA (www.pangaea.de/). Details of the records are given in SI Table S1. The average temporal resolution of these records is 101 years. We then excluded a few samples where the reconstructed values of α exceed the natural limit of 0 and 1.26. Finally, 7214 samples from 117 records are used for the analyses of the climate reconstructions.

In addition to examining the reconstructions for individual sites, we constructed composite curves for the Iberian Peninsula as a whole. The composite curves provide a way of comparing the relationship between trends in the reconstructed climate changes and insolation changes. The curves were constructed after binning the site-based reconstructions using ± 500-year bins.

We did 1000 bootstrap resampling of the reconstructed climate values in each ± 500-year bin to avoid the influence of a single value or a single site on the mean climate value in this bin, and use the standard deviation of the 1000 values to represent the uncertainty of the mean climate value. We constructed linear regression plots to examine the longitudinal and elevational patterns in the reconstructed climate variables, and assessed the significance of differences in these trends through time compared to the most recent bin (0.5 ka ± 500 years) based on *p* values, with the customary threshold of 0.05. We then compared the climate trends with changes in summer and winter insolation.

3. Results

The modified version of fxTWA-PLS reproduces the modern climate reasonably well (Table 1). The performance is best for MTCO (R^2 0.75, RMSEP 4.70, slope 0.91) but is also good for α (R^2 0.68, RMSEP 0.16, slope 0.78) and MTWA (R^2 0.57, RMSEP 3.47, slope 0.71). The correlations between pollen records and each of the three bioclimate variables, as assessed by CCA, were strong for both modern climate data and fossil reconstructions (Table 2). The variance inflation factor scores are all less than 6, so there are no multicollinearity problems (Table 2). Furthermore, the taxa that contribute most strongly to reconstructing colder/warmer or wetter/drier climates show predictable patterns consistent with their known ecological preferences (SI Table S2).

Winters were generally colder than present during the early to mid-Holocene, as shown by the coherent patterns of reconstructed anomalies at individual sites (Fig. 3a, 3d). Here “present” means the most recent pollen bin (0.5 ka ± 500 years). The composite curve also shows a general increase in winter temperatures through time (Fig. 4a), consistent with the trend in winter insolation (Fig. 4d). The composite curve shows that it was ca 4°C cooler than today at 11.5 ka and conditions remained cooler than present until ca 2.5 ka. Winter temperature anomalies show no spatial differentiation between western and eastern Iberia (Table 3, SI Fig. S2). The similarity of the changes compared to present geographically is consistent with the idea that the changes in winter temperature are driven by changes in winter insolation.

Summers were somewhat hotter than present in the west and cooler than present in the east during the early and middle Holocene, as shown by the reconstructed anomalies at individual sites (Fig. 3b, 3e). This west-east difference could not arise if the changes in summer temperatures were a direct reflection of the insolation forcing (Fig. 4e). Indeed, the composite curve shows relatively little change in MTWA (Fig. 4b), confirming that there is no direct relationship to insolation forcing (Fig. 4e).

There is a strong west-east gradient in α at the present day (Fig. 2), with wetter conditions in the west and drier conditions in the east. However, the reconstructed anomalies at individual sites (Fig. 3c, 3f) suggest that west was drier and the east was wetter than present in the mid-Holocene, resulting in a flatter west-east gradient. The west-east gradient is significantly different from present between 9.5 ~ 3.5 ka (Fig. 5, Table 3), implying stronger moisture advection into the continental interior during the mid-Holocene. The change in gradient is seen in both high and low elevation sites (SI Fig. S3). There is also significant change in α with elevation between 9.5 ~ 4.5 ka (Table 3, SI Fig. S4).

Summer temperatures are strongly correlated with changes in α, both in terms of spatial correlations in the modern data set at a European scale and in terms of spatial and temporal correlations the fossil data set from Iberian Peninsula (Fig. 6). The patterns of reconstructed anomalies in MTWA and α at individual sites are also coherent (Fig. 3b, 3c, 3e, 3f), showing drier conditions and hotter summers than present in the west and wetter conditions with cooler summers in the east during the early to mid-Holocene. The west-east gradient in MTWA was significantly different from present between 9.5 and 3.5 ka except 8.5 ka (Table 3, SI Fig. S5), roughly the interval when the gradient in α was also significantly different from present. Again, the change in the east-west gradient is registered at both high and low elevation sites (SI Fig. S6). However, there is no significant change in MTWA with elevation except 8.5 and 7.5 ka (Table 3, SI Fig. S7).

4. Discussion

We have shown that there was a gradual increase in MTCO over the Holocene, both for most of the individual sites represented in the data set and for Iberia as a whole. Colder winters in southern Europe during the mid-Holocene (6 ka) are a feature of many earlier reconstructions (e.g. Cheddadi et al., 1997; Wu et al., 2007). A general warming trend over the Holocene is seen in gridded reconstructions of winter season (December, January, February) temperatures as reconstructed using the modern analogue approach by Mauri et al. (2015), although there is somewhat less millennial-scale variability in these reconstructions (SI Fig. S8). Nevertheless, their reconstructions show a cooling of 3°C in the early Holocene, comparable in magnitude to the ca 4°C cooling at 11.5 ka reconstructed here. Although they show conditions slightly cooler than present persisting up to 1 ka, the differences are very small (ca 0.5°C) after 2 ka, again consistent with our reconstructions of MTCO similar to present by 2.5 ka. Quantitative reconstructions of winter temperature for the 5 terrestrial sites from the Iberian Peninsula in the Kaufman et al. (2020) compilation all show a general trend of winter warming over the Holocene, but the magnitude of the change at some of the individual sites is much larger (ca 10°C) and there is no assessment of the uncertainty on these reconstructions. The composite curve of Kaufman et al. (2020) shows an increasing trend in MTCO through the Holocene although with large uncertainties (SI Fig. S8). In contrast to the consistency of the increasing trend in MTCO during the Holocene between our reconstructions and those of Mauri et al. (2015) and Kaufman et al. (2020), there is no discernible trend in MTCO during the Holocene reconstruction of Tarroso et al. (2016). Indeed, there is no significant change in their MTCO values after ca 9 ka, either for the Peninsula as a whole (SI Fig. S8) or for any of the four sub-regions they considered. Our reconstructed trend in winter temperature is consistent with the changes in insolation forcing at this latitude during the Holocene, and is also consistent with transient climate model simulations of the winter temperature response to changing insolation forcing over the late Holocene in this region (SI Fig. S9). Thus, we suggest that changes in winter temperatures are a direct consequence of insolation forcing.

We have shown that there is no overall trend in MTWA during the Holocene. According to our reconstructions, summer temperatures fluctuated between ca 0.5°C above or below modern temperature. The lack of coherent trend in MTWA is consistent with the gridded reconstructions of summer (June, July, August) temperature in the Mauri et al. (2015) data set and also with the 5 terrestrial sites from Iberia included in the Kaufman et al. (2020) data set. However, the patterns shown in the three data sets are very different from one another. Mauri et al. (2015) suggest the early Holocene was colder than today, and although temperatures similar to today were reached at 9 ka, most of the Holocene was characterised by cooler summers. Kaufman et al. (2020), however, showed warmer than present conditions during the early Holocene although they also show cooler conditions during the later Holocene. The differences between the three data sets probably reflect differences in the number of records used, but the lack of coherency points to there not being a strong, regionally coherent signal of summer temperature changes during the Holocene. Tarroso et al. (2016) also showed no significant changes in MTWA after ca 9 ka (SI Fig. S8).

The chironomid record from Laguna de la Roya covers the late glacial and terminates at 10.5

ka (Muñoz Sobrino et al., 2013). The reconstructed July temperature during the early Holocene is ca 12~13 °C, which is considerably cooler than today at this site. However, the authors caution that these samples have poor analogues and the record should be interpreted with caution. Chironomid-based reconstructions of July temperature at Basa de la Mora (Tarrats et al., 2018), a high elevation site in the Pyrenees, indicate temperatures within ± 0.5° C of the modern during the early to mid-Holocene (10~6 ka), similar to our regional composite reconstructions. However, they show persistently conditions cooler than present by ca 1.5 °C between 4.5 and 2 ka, not seen in our reconstructions. Furthermore, direct comparison of our reconstructions of MTWA at Basa de la Mora (SI Fig. S11) to the chironomid-based reconstructions highlights that the two records show very different trajectories, since the pollen-based reconstruction of this site shows a consistent warming trend throughout the Holocene. Although Tarrats et al. (2018) argue that discrepancies between their temperature reconstructions and pollen-based reconstructions reflects the fact that the vegetation of Iberia, including the mountain areas, is largely driven by moisture changes and perhaps is not a good indicator of temperature, we have shown that there is sufficient information in the pollen records to reconstruct temperature and moisture independently (Table 2, Table S2). Thus, the cause of the differences between the pollen-based and chironomid-based reconstructions at Basa de la Mora is presumably related to methodology. In particular, the chironomid reconstructions use a training data set that does not include samples from the Pyrenees, or indeed the Mediterranean more generally, and may therefore not provide good analogues for Holocene changes at this site.

The lack of a clear trend in MTWA in our reconstructions is not consistent with insolation forcing, which shows a declining trend during the Holocene nor is it consistent with simulated changes in MTWA in transient climate model simulations (see supplementary materials for detailed description) of the summer temperature response to changing insolation forcing over the Holocene in this region (SI Fig. S9). The change in moisture gradient during the mid-Holocene, however, suggests an alternative explanation whereby changes in summer temperature are a response to land-surface feedbacks associated with changes in moisture. Specifically, the observed increased advection of moisture into eastern Iberia would have created wetter conditions there, which in turn would permit increased evapotranspiration, implying less allocation of available net radiation to sensible heating, and resulting in cooler air temperatures. Our reconstructions show that the west-east moisture gradient in mid-Holocene was significantly flatter than the steep moisture gradient today, implying a significant increase in moisture advection into the continental interior during this period. Mauri et al. (2015) also showed that summers were generally wetter than present in the east but drier than present in the west at early to mid-Holocene, supporting the idea of a flatter west-east gradient.

We have shown that stronger moisture advection is not a feature of transient climate model simulations of the Holocene, which may explain why these simulations do not show a strong modification of the insolation-driven changes in summer temperature (Fig. S9). Although the amplitude differs, all of the models show a general decline in summer temperature. The failure of the current generation of climate models to simulate the observed strengthening of moisture transport into Europe and Eurasia during the mid-Holocene has been noted for previous versions of these models (e.g. Bartlein et al., 2017; Mauri et al., 2014) and also shown in Fig. S10. Mauri et al. (2014), for example, showed that climate models participating in the last phase of the Coupled Model Intercomparison Project (CMIP5/PMIP3) were unable to reproduce reconstructed climate patterns over Europe at 6000 yr B.P. and indicated that this resulted from over-sensitivity to changes in insolation forcing and the failure to simulate increased moisture transport into the continent. Bartlein et al. (2017) showed that the CMIP5/PMIP3 models simulated warmer and drier conditions in mid-continental Eurasia at 6000 yr B.P., inconsistent with palaeo-environmental reconstructions from the region, as a result of the simulated reduction in the zonal temperature gradient which resulted in weaker westerly flow and reduced moisture fluxes into the mid-continent. They also pointed out the strong feedback between drier conditions and summer temperatures. The drying of the mid-continent is also a strong feature of the mid-Holocene simulations made with the current generation of CMIP6/PMIP4 models (Brierley et al., 2020). The persistence of these data-model mismatches highlights the need for better modelling of land-surface feedbacks on atmospheric circulation and moisture.

Speleothem oxygen-isotope data from the Iberian Peninsula provide support for our pollen-based reconstructions of changes in the west-east gradient of moisture through the Holocene. The speleothem records show a progressive increase in temperature from the Younger Dryas onwards, although the trend is less marked in the west than the east (Baldini et al., 2019). This warming trend is consistent with our reconstructions of changes in MTCO through the Holocene. Speleothem records also show distinctly different patterns in moisture availability, with sites in western Iberia indicating wetter environments during early Holocene and a transition to drier conditions from ca 7.5 cal ka BP to the present (Stoll et al., 2013; Thatcher et al., 2020) while eastern sites record wetter conditions persisting from 9 to 4 cal ka (Walczak et al., 2015). This finding would support the weaker west to east moisture gradient shown by our results.

Pollen data are widely used for the quantitative reconstruction of past climates (see discussion in Bartlein et al., 2011). Nevertheless, climate is not the only driver of vegetation changes. On glacial-interglacial timescales, changes in CO_2 have a direct impact on plant physiological processes and reductions in plant water-use efficiency at low CO_2 result in vegetation appearing to reflect drier conditions than were experienced in reality (Farquhar, 1997; Gerhart and Ward, 2010; Prentice et al., 2017; Prentice and Harrison, 2009). The difference between post- and pre-industrial CO_2 levels could also influence the reliability of moisture reconstructions based on modern training data sets. However, the change in CO_2 over the Holocene was only 40 ppm. Prentice et al. (2022) shows that this change relative to modern levels has only a small impact on pollen-based reconstructed moisture indices. The magnitude of this impact is within the uncertainties on our reconstructions. Furthermore, accounting for the effect of this change in CO_2 or not won't affect the reconstructed west-east gradient through time. Therefore, we have not accounted for the impact of changing CO_2 in our reconstructions of α, although there are techniques to do this (Prentice et al., 2011, 2017; Wei et al., 2021). A more serious issue for our reconstructions may be the extent to which the vegetation cover of Iberia was substantially modified by human activities during the Holocene. While there is no doubt that anthropogenic activities were important at the local scale and particularly in the later Holocene (e.g. Abel-Schaad and López-Sáez, 2013; Connor et al., 2019; Fyfe et al., 2019; Mighall et al., 2006; Revelles et al., 2015), most of the sites used for our reconstructions are not associated with archaeological evidence of agriculture or substantial landscape modification. Furthermore, the consistency of the reconstructed changes in climate across sites provides support for these being largely a reflection of regional climate changes.

We have used a modified version of fxTWA-PLS to reconstruct Holocene climates of the Iberian Peninsula because this modification reduced the compression bias in MTCO and MTWA, and specifically reduces the maximum bias in MTCO, MTWA and α. Although this modified approach produces better overall reconstructions (Appendix A), its use does not change the reconstructed trends in these variables through time (SI Fig. S12). Thus, the finding that winter temperatures are a direct reflection of insolation forcing whereas summer temperatures are influenced by land-surface feedbacks and changes in atmospheric circulation is robust to the method used. However, while we use a much larger data set than previous reconstructions, the distribution of pollen sites is uneven and the northern part of the Peninsula is better sampled than the southwest, which could lead to some uncertainties in the interpretation of changes in the west-east gradient of moisture. It would, therefore, be useful to specifically target the southwestern part of the Iberian Peninsula for new data collection. Alternatively, it would be useful to apply the approach used here to the whole of Eurasia, given that the failure of state-of-the-art climate models to advect moisture into the continental interior appears to be a feature of the whole region (Bartlein et al., 2017) and not the Peninsula alone.

5. Conclusion

We have used a pollen data set representing 117 sites across the Iberian Peninsula to make quantitative reconstructions of summer and winter temperature and an index of annual moisture through the Holocene. We show that the trends in winter temperature broadly follow the changes orbital forcing. Summer temperatures, however, do not follow the changes in orbital forcing but appear to be influenced by land-surface feedbacks associated with changes in moisture. The west-east gradient in moisture was considerably less pronounced during the mid-Holocene (8-4 ka).

Data and Code Availability

All the data used are public access and cited here. The code used to generate the climate reconstructions is available at https://github.com/ml4418/Iberia-paper.git.

Supplement. The supplement related to this article is available online.

Competing interests. We declare that we have no conflict of interest.

Author Contributions. ML, ICP and SPH designed the study. ML, ICP and CJFtB designed the modifications to fxTWA-PLS. PG-S and GG-R provided pollen data and insights into the regional palaeoclimate histories. ML carried out the analyses. ML and SPH wrote the first draft of the paper and all authors contributed to the final draft.

Acknowledgements. ML acknowledges support from Imperial College through the Lee Family Scholarship. YS and SPH acknowledge support from the ERC-funded project GC 2.0 (Global Change 2.0: Unlocking the past for a clearer future; grant number 694481). ICP acknowledges support from the ERC under the European Union Horizon 2020 research and innovation programme (grant agreement no: 787203 REALM). This work is a contribution to the project "Origen y Cuantification de los Cambios Paleoambientales en el Pirineo: Variabilidad climatic e impacto humano" (PYCACHU: PID2019-106050RB-I00)" funded by the Ministerio de Ciencia e Innovación.

Financial support. This research has been supported by Lee Family Scholarship fund, and the European Research Council (grant no. GC2.0, 694481, and grant no. REALM, 787203).

References

Abel-Schaad, D., López-Sáez, J.A.: Vegetation changes in relation to fire history and human activities at the Peña Negra mire (Bejar Range, Iberian Central Mountain System, Spain) during the past 4,000 years. Veg. Hist. Archaeobot. 22, 199–214. https://doi.org/10.1007/s00334-012-0368-9, 2013.

Abel-Schaad, D. and López-Sáez, J. A.: Vegetation changes in relation to fire history and human activities at the Peña Negra mire (Bejar Range, Iberian Central Mountain System, Spain) during the past 4,000 years, Veg. Hist. Archaeobot., 22, 199–214, doi:10.1007/s00334-012-0368-9, 2013.

Andrade, C., Contente, J. and Santos, J. A.: Climate change projections of aridity conditions in the Iberian Peninsula, Water, 13(15), doi:10.3390/w13152035, 2021a.

Andrade, C., Contente, J. and Santos, J. A.: Climate change projections of dry and wet events in Iberia based on the WASP-Index, Climate, 9(6), doi:10.3390/cli9060094, 2021b.

Aranbarri, J., Gonzalez Samperiz, P., Valero-Garcés, B., Moreno, A., Gil-Romera, G., Sevilla-Callejo, M., Garcia-Prieto, E., Di Rita, F., Mata, M. del Pi., Morellón, M., Magri, D., Rodriguez-Lazaro, J. and Carrión, J.: Rapid climatic changes and resilient vegetation during the Lateglacial and Holocene in a continental region of south-western Europe, Glob. Planet. Change, 114, 50–65, doi:10.1016/j.gloplacha.2014.01.003, 2014.

Aranbarri, J., González-Sampériz, P., Iriarte, E., Moreno, A., Rojo-Guerra, M., Peña-Chocarro, L., Valero-Garcés, B., Leunda, M., García-Prieto, E., Sevilla-Callejo, M., Gil-Romera, G., Magri, D. and Rodríguez-Lázaro, J.: Human–landscape interactions in the Conquezuela–Ambrona Valley (Soria, continental Iberia): From the early Neolithic land use to the origin of the current oak woodland, Palaeogeogr. Palaeoclimatol. Palaeoecol., 436, 41–57, doi:https://doi.org/10.1016/j.palaeo.2015.06.030, 2015.

Baldini, L. M., Baldini, J. U. L., McDermott, F., Arias, P., Cueto, M., Fairchild, I. J., Hoffmann, D. L., Mattey, D. P., Müller, W., Nita, D. C., Ontañón, R., Garciá-Moncó, C. and Richards, D. A.: North Iberian temperature and rainfall seasonality over the Younger Dryas and Holocene, Quat. Sci. Rev., 226, 105998, doi:https://doi.org/10.1016/j.quascirev.2019.105998, 2019.

Bartlein, P. J., Prentice, I. C. and Webb, T.: Climatic response surfaces from pollen data for some Eastern North American taxa, J. Biogeogr., 13(1), 35, doi:10.2307/2844848, 1986.

Bartlein, P. J., Harrison, S. P., Brewer, S., Connor, S., Davis, B. A. S., Gajewski, K., Guiot, J., Harrison-Prentice, T. I., Henderson, A., Peyron, O., Prentice, I. C., Scholze, M., Seppä, H., Shuman, B., Sugita, S., Thompson, R. S., Viau, A. E., Williams, J. and Wu, H.: Pollen-based continental climate reconstructions at 6 and 21 ka: A global synthesis, Clim. Dyn., 37(3), 775–802, doi:10.1007/s00382-010-0904-1, 2011.

Bartlein, P. J., Harrison, S. P. and Izumi, K.: Underlying causes of Eurasian midcontinental aridity in simulations of mid-Holocene climate, Geophys. Res. Lett., 44(17), 9020–9028, doi:10.1002/2017GL074476, 2017.

Blaauw, M. and Christeny, J. A.: Flexible paleoclimate age-depth models using an autoregressive gamma process, Bayesian Anal., 6(3), 457–474, doi:10.1214/11-BA618, 2011.

Blaauw, M., Christen, J. A., Lopez, M. A. A. V., V., J. E. O. M. G., Belding, T., Theiler, J., Gough, B. and Karney, C.: rbacon: Age-depth modelling using Bayesian statistics, [online] Available from: https://cran.r-project.org/package=rbacon, 2021.

ter Braak, C. J. F. and Juggins, S.: Weighted averaging partial least squares regression (WA-PLS): An improved method for reconstructing environmental variables from species assemblages, Hydrobiologia, 269(1), 485–502, doi:10.1007/BF00028046, 1993.

Brierley, C. M., Zhao, A., Harrison, S. P., Braconnot, P., Williams, C. J. R., Thornalley, D. J. R., Shi, X., Peterschmitt, J.-Y., Ohgaito, R., Kaufman, D. S., Kageyama, M., Hargreaves, J. C., Erb, M. P., Emile-Geay, J., D'Agostino, R., Chandan, D., Carré, M., Bartlein, P., Zheng, W., Zhang, Z., Zhang, Q., Yang, H., Volodin, E. M., Tomas, R. A., Routson, C., Peltier, W. R., Otto-Bliesner, B., Morozova, P. A., McKay, N. P., Lohmann, G., Legrande, A. N., Guo, C., Cao, J., Brady, E., Annan, J. D. and Abe-Ouchi, A.: Large-scale features and evaluation of the PMIP4-CMIP6 midHolocene simulations, Clim. Past Discuss., 2020, 1–35, doi:10.5194/cp-2019-168, 2020.

Carrión, J. S., Fernández, S., González-Sampériz, P., Gil-Romera, G., Badal, E., Carrión-Marco, Y., López-Merino, L., López-Sáez, J. A., Fierro, E. and Burjachs, F.: Expected trends and surprises in the Lateglacial and Holocene vegetation history of the Iberian Peninsula and Balearic Islands, Rev. Palaeobot. Palynol., 162(3), 458–475, doi:https://doi.org/10.1016/j.revpalbo.2009.12.007, 2010.

Carrión, Y., Kaal, J., López-Sáez, J. A., López-Merino, L. and Martínez Cortizas, A.: Holocene vegetation changes in NW Iberia revealed by anthracological and palynological records from a colluvial soil, The Holocene, 20(1), 53–66, doi:10.1177/0959683609348849, 2009.

Carvalho, D., Pereira, S. and Rocha, A.: Future surface temperature changes for the Iberian Peninsula according to EURO-CORDEX climate projections, Clim. Dyn., 56, 1–16, doi:10.1007/s00382-020-05472-3, 2021.

Cheddadi, R., Yu, G., Joel, G., Harrison, S., Prentice, I. and Colin, I.: The climate of Europe 6000 years ago, cd, 13, 1, doi:10.1007/s003820050148, 1997.

Chevalier, M., Davis, B. A. S., Heiri, O., Seppä, H., Chase, B. M., Gajewski, K., Lacourse, T., Telford, R. J., Finsinger, W., Guiot, J., Kühl, N., Maezumi, S. Y., Tipton, J. R., Carter, V. A., Brussel, T., Phelps, L. N., Dawson, A., Zanon, M., Vallé, F., Nolan, C., Mauri, A., de Vernal, A., Izumi, K., Holmström, L., Marsicek, J., Goring, S., Sommer, P. S., Chaput, M. and Kupriyanov, D.: Pollen-based climate reconstruction techniques for late Quaternary studies, Earth-Science Rev., 210, 103384, doi:https://doi.org/10.1016/j.earscirev.2020.103384, 2020.

Connor, S., Vannière, B., Colombaroli, D., Anderson, R., Carrión, J., Ejarque, A., Gil-Romera, G., Gonzalez Samperiz, P., Höfer, D., Morales-Molino, C., Revelles, J., Schneider, H., Knaap, W., Leeuwen, J. and Woodbridge, J.: Humans take control of fire-driven diversity changes in Mediterranean Iberia's vegetation during the mid–late Holocene, The Holocene, 29, 095968361982665, doi:10.1177/0959683619826652, 2019.

Davis, T. W., Prentice, I. C., Stocker, B. D., Thomas, R. T., Whitley, R. J., Wang, H., Evans, B. J., Gallego-Sala, A. V, Sykes, M. T. and Cramer, W.: Simple process-led algorithms for simulating habitats (SPLASH v.1.0): Robust indices of radiation, evapotranspiration and plant-available moisture, Geosci. Model Dev., 10(2), 689–708, doi:10.5194/gmd-10-689-2017, 2017.

Eilers, P. H. and Marx, B. D.: Practical smoothing: The Joys of P-splines, edited by P. H. Eilers and B. D. Marx, Cambridge University Press., 2021.

Farquhar, G. D.: Carbon dioxide and vegetation, Science (80-.)., 278(5342), 1411, doi:10.1126/science.278.5342.1411, 1997.

Fyfe, R. M., Woodbridge, J., Palmisano, A., Bevan, A., Shennan, S., Burjachs, F., Legarra Herrero, B., García Puchol, O., Carrión, J. S., Revelles, J. and Roberts, C. N.: Prehistoric palaeodemographics and regional land cover change in eastern Iberia, Holocene, 29(5), 799–815, doi:10.1177/0959683619826643, 2019.

Gerhart, L. M. and Ward, J. K.: Plant responses to low [CO_2] of the past, New Phytol., 188(3), 674–695, doi:https://doi.org/10.1111/j.1469-8137.2010.03441.x, 2010.

González-Sampériz, P., Aranbarri, J., Pérez-Sanz, A., Gil-Romera, G., Moreno, A., Leunda, M., Sevilla-Callejo, M., Corella, J. P., Morellón, M., Oliva, B. and Valero-Garcés, B.: Environmental and climate change in the southern Central Pyrenees since the Last Glacial Maximum: A view from the lake records, Catena, 149, 668–688, doi:https://doi.org/10.1016/j.catena.2016.07.041, 2017.

Granados, I. and Toro, M.: Recent warming in a high mountain lake (Laguna Cimera, Central Spain) inferred by means of fossil chironomids, J. Limnol., 59 (suppl., 109–119, doi:10.4081/jlimnol.2000.s1.109, 2000.

Harrison, S., Shen, Y. and Sweeney, L.: Pollen data and charcoal data of the Iberian Peninsula (version 3), [online] Available from: https://doi.org/10.17864/1947.000369, 2022.

Harrison, S. P.: Modern pollen data for climate reconstructions, version 1 (SMPDS), , doi:http://dx.doi.org/10.17864/1947.194, 2019.

Holden, P. B., Birks, H. J. B., Brooks, S. J., Bush, M. B., Hwang, G. M., Matthews-Bird, F., Valencia, B. G. and van Woesik, R.: BUMPER v1.0: a Bayesian user-friendly model for palaeo-environmental reconstruction, Geosci. Model Dev., 10(1), 483–498, doi:10.5194/gmd-10-483-2017, 2017.

Kaufman, D., McKay, N., Routson, C., Erb, M., Davis, B., Heiri, O., Jaccard, S., Tierney, J., Dätwyler, C., Axford, Y., Brussel, T., Cartapanis, O., Chase, B., Dawson, A., de Vernal, A., Engels, S., Jonkers, L., Marsicek, J., Moffa-Sánchez, P., Morrill, C., Orsi, A., Rehfeld, K., Saunders, K., Sommer, P. S., Thomas, E., Tonello, M., Tóth, M., Vachula, R., Andreev, A., Bertrand, S., Biskaborn, B., Bringué, M., Brooks, S., Caniupán, M., Chevalier, M., Cwynar, L., Emile-Geay, J., Fegyveresi, J., Feurdean, A., Finsinger, W., Fortin, M.-C., Foster, L., Fox, M., Gajewski, K., Grosjean, M., Hausmann, S., Heinrichs, M., Holmes, N., Ilyashuk, B., Ilyashuk, E., Juggins, S., Khider, D., Koinig, K., Langdon, P., Larocque-Tobler, I., Li, J., Lotter, A., Luoto, T., Mackay, A., Magyari, E., Malevich, S., Mark, B., Massaferro, J., Montade, V., Nazarova, L., Novenko, E., Pařil, P., Pearson, E., Peros, M., Pienitz, R., Płóciennik, M., Porinchu, D., Potito, A., Rees, A., Reinemann, S., Roberts, S., Rolland, N., Salonen, S., Self, A., Seppä, H., Shala, S., St-Jacques, J.-M., Stenni, B., Syrykh, L., Tarrats, P., Taylor, K., van den Bos, V., Velle, G., Wahl, E., Walker, I., Wilmshurst, J., Zhang, E. and Zhilich, S.: A global database of Holocene paleotemperature records, Sci. Data, 7(1), 115, doi:10.1038/s41597-020-0445-3, 2020.

Liu, M., Prentice, I. C., ter Braak, C. J. F. and Harrison, S. P.: An improved statistical approach for reconstructing past climates from biotic assemblages, Proc. R. Soc. A Math., 476(2243), doi:https://doi.org/10.1098/rspa.2020.0346, 2020.

Martínez-Cortizas, A., Costa-Casais, M. and López-Sáez, J. A.: Environmental change in NW Iberia between 7000 and 500cal BC, Quat. Int., 200(1), 77–89, doi:https://doi.org/10.1016/j.quaint.2008.07.012, 2009.

Mauri, A., Davis, B. A. S., Collins, P. M. and Kaplan, J. O.: The influence of atmospheric circulation on the mid-Holocene climate of Europe: a data–model comparison, Clim. Past, 10(5), 1925–1938, doi:10.5194/cp-10-1925-2014, 2014.

Mauri, A., Davis, B. A. S., Collins, P. M. and Kaplan, J. O.: The climate of Europe during the Holocene: A gridded pollen-based reconstruction and its multi-proxy evaluation, Quat. Sci. Rev., 112, 109–127, doi:10.1016/j.quascirev.2015.01.013, 2015.

Mighall, T. M., Martínez Cortizas, A., Biester, H. and Turner, S. E.: Proxy climate and vegetation changes during the last five millennia in NW Iberia: Pollen and non-pollen palynomorph data from two ombrotrophic peat bogs in the North Western Iberian Peninsula, Rev. Palaeobot. Palynol., 141(1–2), 203–223, doi:10.1016/j.revpalbo.2006.03.013, 2006.

Millet, L., Rius, D., Galop, D., Heiri, O. and Brooks, S. J.: Chironomid-based reconstruction of Lateglacial summer temperatures from the Ech palaeolake record (French western Pyrenees), Palaeogeogr. Palaeoclimatol. Palaeoecol., 315–316, 86–99, doi:https://doi.org/10.1016/j.palaeo.2011.11.014, 2012.

Morellón, M., Aranbarri, J., Moreno, A., González-Sampériz, P. and Valero-Garcés, B. L.: Early Holocene humidity patterns in the Iberian Peninsula reconstructed from lake, pollen and speleothem records, Quat. Sci. Rev., 181, 1–18, doi:https://doi.org/10.1016/j.quascirev.2017.11.016, 2018.

Muñoz Sobrino, C., Heiri, O., Hazekamp, M., van der Velden, D., Kirilova, E. P., García-Moreiras, I. and Lotter, A. F.: New data on the Lateglacial period of SW Europe: a high resolution multiproxy record from Laguna de la Roya (NW Iberia), Quat. Sci. Rev., 80, 58–77, doi:https://doi.org/10.1016/j.quascirev.2013.08.016, 2013.

New, M., Lister, D. and Hulme, M.: A high-resolution data set of surface climate over global land areas , Clim. Res., 21(1), 1–25 [online] Available from: http://www.int-res.com/abstracts/cr/v21/n1/p1-25/, 2002.

Overpeck, J. T., Webb, T. and Prentice, I. C.: Quantitative interpretation of fossil pollen spectra: Dissimilarity coefficients and the method of modern analogs, Quat. Res., 23(1), 87–108, doi:10.1016/0033-5894(85)90074-2, 1985.

Peyron, O., Guiot, J., Cheddadi, R., Tarasov, P., Reille, M., de Beaulieu, J.-L., Bottema, S. and Andrieu, V.: Climatic reconstruction in Europe for 18,000 yr B.P. from pollen data, Quat. Res., 49(2), 183–196, doi:https://doi.org/10.1006/qres.1997.1961, 1998.

Prentice, I. C. and Harrison, S. P.: Ecosystem effects of CO_2 concentration: evidence from past climates, Clim. Past, 5(3), 297–307, doi:10.5194/cp-5-297-2009, 2009.

Prentice, I. C., Meng, T., Wang, H., Harrison, S. P., Ni, J. and Wang, G.: Evidence of a universal scaling relationship for leaf CO2 drawdown along an aridity gradient, New Phytol., 190(1), 169–180, doi:https://doi.org/10.1111/j.1469-8137.2010.03579.x, 2011.

Prentice, I. C., Cleator, S. F., Huang, Y. H., Harrison, S. P. and Roulstone, I.: Reconstructing ice-age palaeoclimates: Quantifying low-CO_2 effects on plants, Glob. Planet. Change, 149, 166–176, doi:https://doi.org/10.1016/j.gloplacha.2016.12.012, 2017.

Prentice, I. C., Villegas-Diaz, R. and Harrison, S. P.: Accounting for atmospheric carbon dioxide variations in pollen-based reconstruction of past hydroclimates, Glob. Planet. Change, 2022.

Reimer, P. J., Austin, W. E. N., Bard, E., Bayliss, A., Blackwell, P. G., Bronk Ramsey, C., Butzin, M., Cheng, H., Edwards, R. L., Friedrich, M., Grootes, P. M., Guilderson, T. P., Hajdas, I., Heaton, T. J., Hogg, A. G., Hughen, K. A., Kromer, B., Manning, S. W., Muscheler, R., Palmer, J. G., Pearson, C., Van Der Plicht, J., Reimer, R. W., Richards, D. A., Scott, E. M., Southon, J. R., Turney, C. S. M., Wacker, L., Adolphi, F., Büntgen, U., Capano, M., Fahrni, S. M., Fogtmann-Schulz, A., Friedrich, R., Köhler, P., Kudsk, S., Miyake, F., Olsen, J., Reinig, F., Sakamoto, M., Sookdeo, A. and Talamo, S.: The IntCal20 Northern Hemisphere radiocarbon age calibration curve (0-55 cal kBP), Radiocarbon, 62(4), 725–757, doi:10.1017/RDC.2020.41, 2020.

Revelles, J., Cho, S., Iriarte, E., Burjachs, F., van Geel, B., Palomo, A., Piqué, R., Peña-Chocarro, L. and Terradas, X.: Mid-Holocene vegetation history and Neolithic land-use in the Lake Banyoles area (Girona, Spain), Palaeogeogr. Palaeoclimatol. Palaeoecol., 435, 70–85, doi:10.1016/j.palaeo.2015.06.002, 2015.

Salonen, J. S., Ilvonen, L., Seppä, H., Holmström, L., Telford, R. J., Gaidamavičius, A., Stančikaitė, M. and Subetto, D.: Comparing different calibration methods (WA/WA-PLS regression and Bayesian modelling) and different-sized calibration sets in pollen-based quantitative climate reconstruction, The Holocene, 22(4), 413–424, doi:10.1177/0959683611425548, 2011.

Shen, Y., Sweeney, L., Liu, M., Lopez Saez, J. A., Pérez-Díaz, S., Luelmo-Lautenschlaeger, R., Gil-Romera, G., Hoefer, D., Jiménez-Moreno, G., Schneider, H., Prentice, I. C. and Harrison, S. P.: Reconstructing burnt area during the Holocene: an Iberian case study, Clim. Past Discuss., 2021, 1–23, doi:10.5194/cp-2021-36, 2021.

Stoll, H. M., Moreno, A., Mendez-Vicente, A., Gonzalez-Lemos, S., Jimenez-Sanchez, M., Dominguez-Cuesta, M. J., Edwards, R. L., Cheng, H. and Wang, X.: Paleoclimate and growth rates of speleothems in the northwestern Iberian Peninsula over the last two glacial cycles, Quat. Res., 80, 284–290, doi:10.1016/j.yqres.2013.05.002, 2013.

Tarrats, P., Heiri, O., Valero-Garcés, B., Cañedo-Argüelles, M., Prat, N., Rieradevall, M. and González-Sampériz, P.: Chironomid-inferred Holocene temperature reconstruction in Basa de la Mora Lake (Central Pyrenees), The Holocene, 28(11), 1685–1696, doi:10.1177/0959683618788662, 2018.

Tarroso, P., Carrión, J., Dorado-Valiño, M., Queiroz, P., Santos, L., Valdeolmillos-Rodríguez, A., Célio Alves, P., Brito, J. C. and Cheddadi, R.: Spatial climate dynamics in the Iberian Peninsula since 15 000 yr BP, Clim. Past, 12(5), 1137–1149, doi:10.5194/cp-12-1137-2016, 2016.

Thatcher, D. L., Wanamaker, A. D., Denniston, R. F., Asmerom, Y., Polyak, V. J., Fullick, D., Ummenhofer, C. C., Gillikin, D. P. and Haws, J. A.: Hydroclimate variability from western Iberia (Portugal) during the Holocene: Insights from a composite stalagmite isotope record, The Holocene, 30(7), 966–981, doi:https://doi.org/10.1177/0959683620908648, 2020.

Villegas-Diaz, Roberto; Cruz-Silva, Esmeralda; Harrison, S. P.: ageR: Supervised age models, , doi:10.5281/zenodo.4636715, 2021.

Walczak, I. W., Baldini, J. U. L., Baldini, L. M., McDermott, F., Marsden, S., Standish, C. D., Richards, D. A., Andreo, B. and Slater, J.: Reconstructing high-resolution climate using CT scanning of unsectioned stalagmites: A case study identifying the mid-Holocene onset of the Mediterranean climate in southern Iberia, Quat. Sci. Rev., 127, 117–128, doi:https://doi.org/10.1016/j.quascirev.2015.06.013, 2015.

Wei, D., González-Sampériz, P., Gil-Romera, G., Harrison, S. P. and Prentice, I. C.: Seasonal temperature and moisture changes in interior semi-arid Spain from the last interglacial to the Late Holocene, Quat. Res., 101, 143–155, doi:DOI: 10.1017/qua.2020.108, 2021.

Wu, H., Guiot, J., Brewer, S. and Guo, Z.: Climatic changes in Eurasia and Africa at the last glacial maximum and mid-Holocene: reconstruction from pollen data using inverse vegetation modelling, Clim. Dyn., 29(2), 211–229, doi:10.1007/s00382-007-0231-3, 2007.

Figure and Table Captions

Figure 1. Climate space represented by mean temperature of the coldest month (MTCO), mean temperature of the warmest month (MTWA), and plant-available moisture as represented by α, an estimate of the ratio of actual evapotranspiration to equilibrium evapotranspiration. The grey points show climate values for a rectangular area (21° W ~ 150° E, 29° N ~ 82° N) enclosing the SMPDS data set, derived from the Climate Research Unit CRU CL 2.0 database (New et al., 2002). The black points show climate values of the SMPDS dataset. The red points show climate values of the Iberian Peninsula region in the SMPDS dataset.

Figure 2. Map showing the location of the 117 fossil sites in the Iberian Peninsula used for climate reconstructions. Sites lower than 1000 m above sea level are shown as squares, sites higher than 1000 m above sea level are shown as triangles. The base maps show modern (a) mean temperature of the coldest month (MTCO), (b) mean temperature of the warmest month (MTWA), and (c) plant-available moisture as represented by α, an estimate of the ratio of actual evapotranspiration to equilibrium evapotranspiration.

Figure 3. Reconstructed anomalies in climate at individual sites through time. The sites are grouped into high (>1000m) and low (<1000m) elevation sites and organised from west to east. Grey cells indicate periods or longitudes with no data. The individual plots show the anomalies in reconstructed (a,d) mean temperature of the coldest month (MTCO), (b,e) mean temperature of the warmest month (MTWA), and (c,f) plant-available moisture as represented by α, an estimate of the ratio of actual evapotranspiration to equilibrium evapotranspiration. The anomalies are expressed as deviations of the mean value in each bin (± 500 years) from the value at 0.5 ka at each site.

Figure 4. Reconstructed composite changes (anomalies to 0.5 ka) in (a) mean temperature of the coldest month (MTCO), (b) mean temperature of the warmest month (MTWA) and (c) plant-available moisture as represented by α, through the Holocene compared to changes in (d) winter and (e) summer insolation for the latitude of the Iberian Peninsula, using ± 500 years as the bin. The black lines show mean values across sites, with vertical line segments showing the standard deviations of mean values using 1000 bootstrap cycles of site resampling.

Figure 5. Changes in the west-east gradient of plant-available moisture as represented by anomalies in α relative to 0.5 ka at individual sites through the Holocene. The red lines show the regression lines. The shades indicate the 95 % confidence intervals of the regression lines

Figure 6. The relationship between mean temperature of the warmest month (MTWA) and plant-available moisture as represented by α (a) in the modern climate data set, and (b) in the Holocene reconstructions.

Table 1. Leave-out cross-validation (with geographically and climatically close sites removed) fitness of the modified version of fxTWA-PLS, for mean temperature of the coldest month (MTCO), mean temperature of the warmest month (MTWA) and plant-available moisture (α), with p-spline smoothed fx estimation, using bins of 0.02, 0.02 and 0.002, showing results for all the components. RMSEP is the root-mean-square error of prediction. ΔRMSEP is the per cent change of RMSEP using the current number of components than using one component less. p assesses whether using the current number of components is significantly different from using one component less, which is used to choose the last significant number of components (indicated in bold) to avoid over-fitting. The degree of overall compression is assessed by linear regression of the cross-validated reconstructions onto the climate variable, b1, b1.se are the slope and the standard error of the slope, respectively. The closer the slope (b1) is to 1, the less the overall compression is.

Table 2. Canonical Correspondence Analysis (CCA) result of modern and fossil-reconstructed MTCO, MTWA and α. The summary statistics for the ANOVA-like permutation test (999 permutations) are also shown. VIF is the variance inflation factor, Df is the number of degrees of freedom, χ^2 is the constrained eigenvalue (or the sum of constrained eigenvalues for the whole model), F is significance, and Pr (>F) is the probability.

Table 3. Assessment of the significance of anomalies to 0.5 ka through time with latitude and elevation. The slope is obtained by linear regression of the anomaly onto the longitude or elevation. p is the significance of the slope (bold parts: $p < 0.05$). x_0 is the point where the anomaly is 0 in the linear equation, which indicates longitude or elevation where the anomaly changes sign.

Figure 1. Climate space represented by mean temperature of the coldest month (MTCO), mean temperature of the warmest month (MTWA), and plant-available moisture as represented by α, an estimate of the ratio of actual evapotranspiration to equilibrium evapotranspiration. The grey points show climate values for a rectangular area (21° W ~ 150° E, 29° N ~ 82° N) enclosing the SMPDS data set, derived from the Climate Research Unit CRU CL 2.0 database (New et al., 2002). The black points show climate values of the SMPDS dataset. The red points show climate values of the Iberian Peninsula region in the SMPDS dataset.

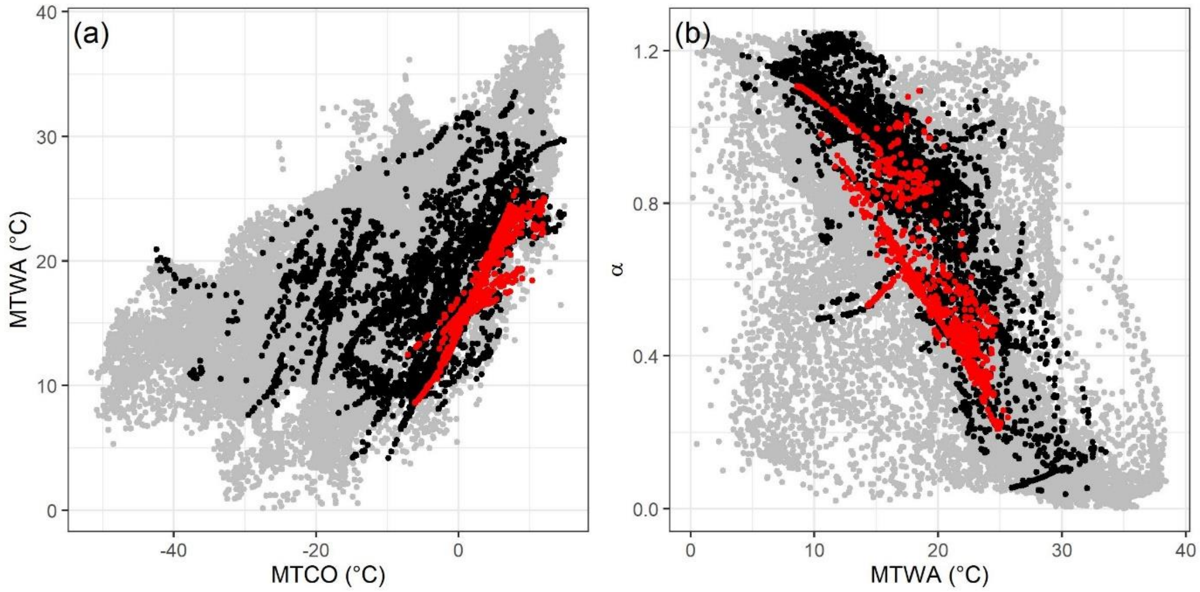

Figure 2. Map showing the location of the 117 fossil sites in the Iberian Peninsula used for climate reconstructions. Sites lower than 1000 m above sea level are shown as squares, sites higher than 1000 m above sea level are shown as triangles. The base maps show modern (a) mean temperature of the coldest month (MTCO), (b) mean temperature of the warmest month (MTWA), and (c) plant-available moisture as represented by α, an estimate of the ratio of actual evapotranspiration to equilibrium evapotranspiration.

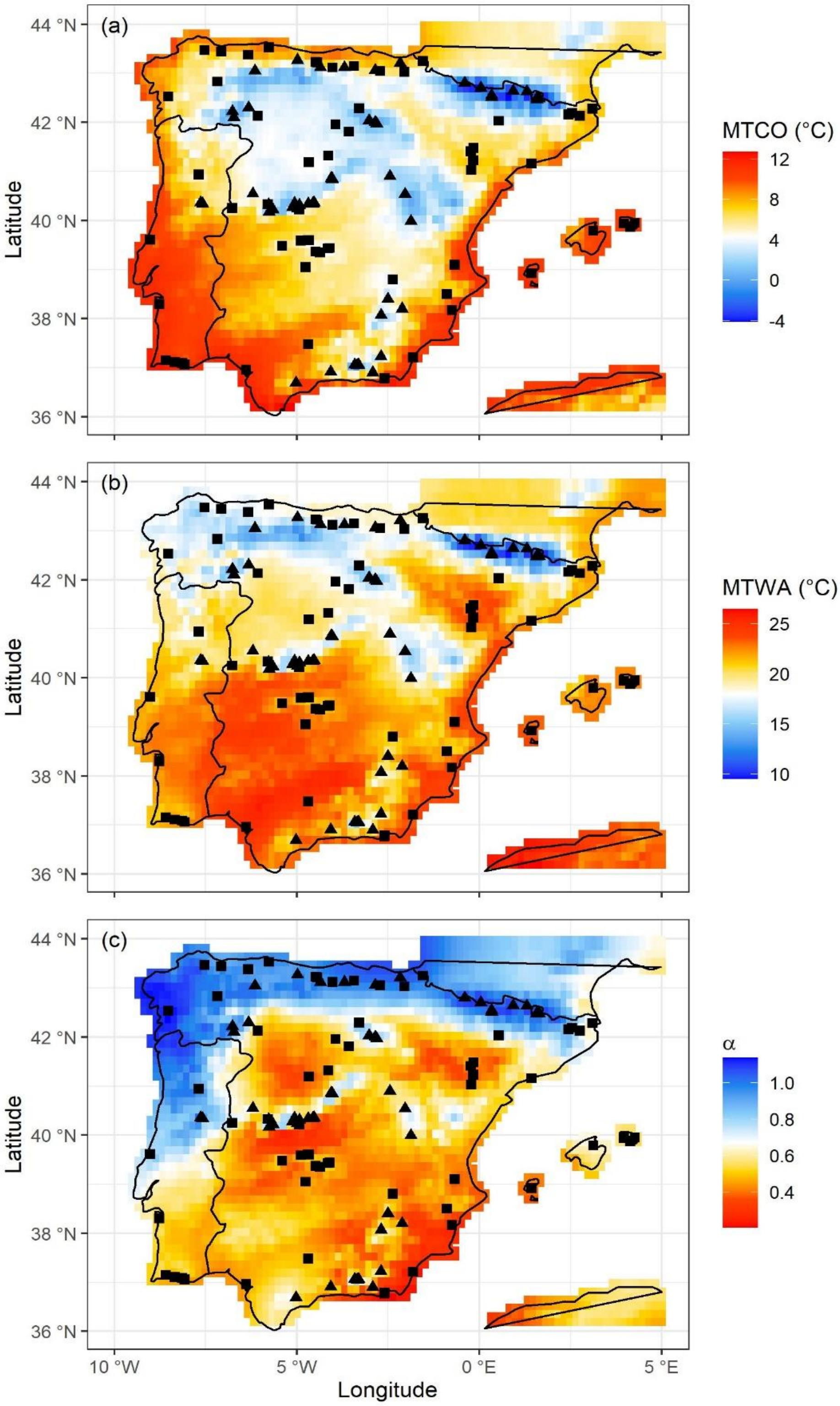

Figure 3. Reconstructed anomalies in climate at individual sites through time. The sites are grouped into high (>1000m) and low (<1000m) elevation sites and organised from west to east. Grey cells indicate periods or longitudes with no data. The individual plots show the anomalies in reconstructed (a,d) mean temperature of the coldest month (MTCO), (b,e) mean temperature of the warmest month (MTWA), and (c,f) plant-available moisture as represented by α, an estimate of the ratio of actual evapotranspiration to equilibrium evapotranspiration. The anomalies are expressed as deviations of the mean value in each bin (± 500 years) from the value at 0.5 ka at each site.

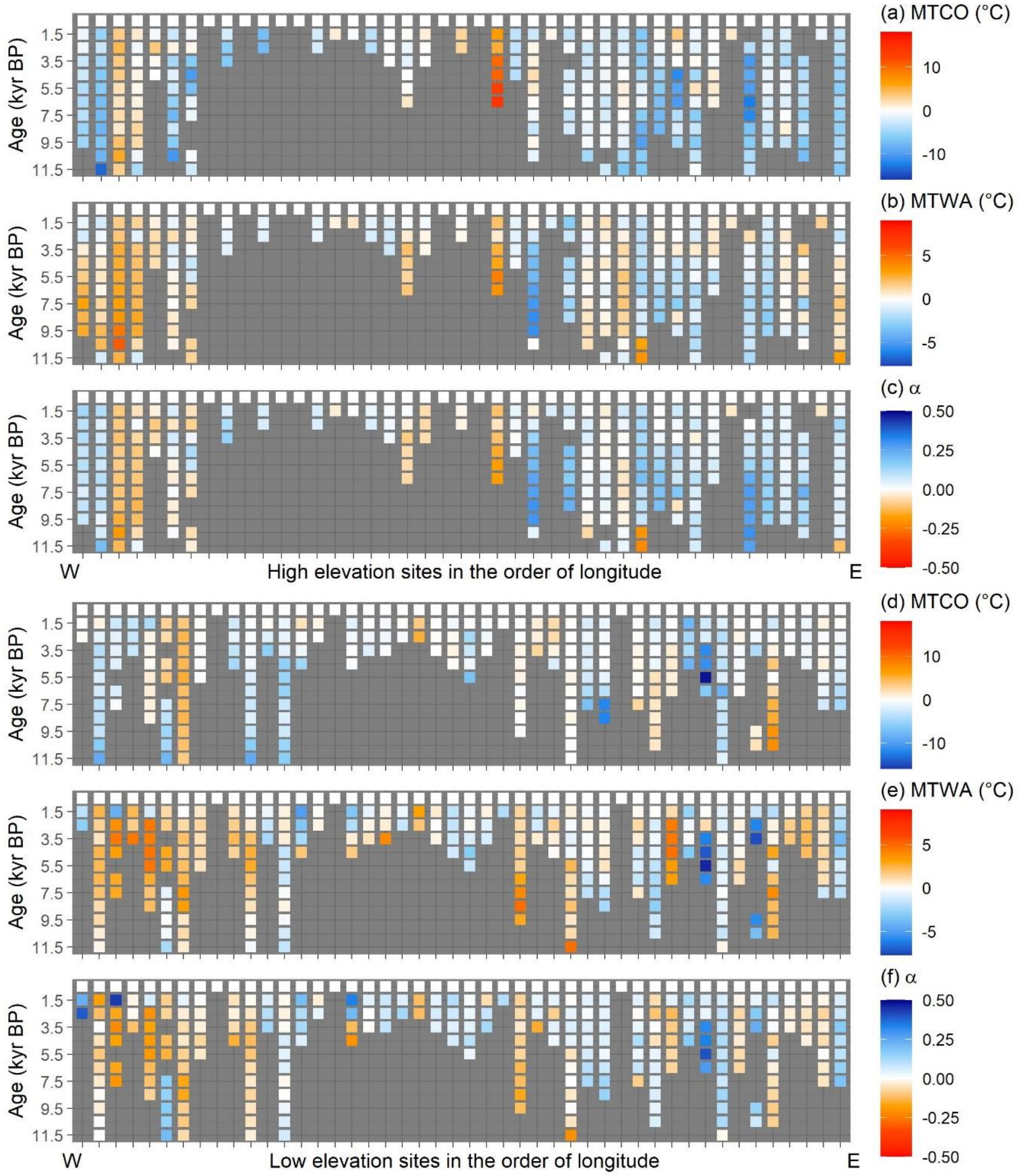

Figure 4. Reconstructed composite changes (anomalies to 0.5 ka) in (a) mean temperature of the coldest month (MTCO), (b) mean temperature of the warmest month (MTWA) and (c) plant-available moisture as represented by α, through the Holocene compared to changes in (d) winter and (e) summer insolation for the latitude of the Iberian Peninsula, using ± 500 years as the bin. The black lines show mean values across sites, with vertical line segments showing the standard deviations of mean values using 1000 bootstrap cycles of site resampling.

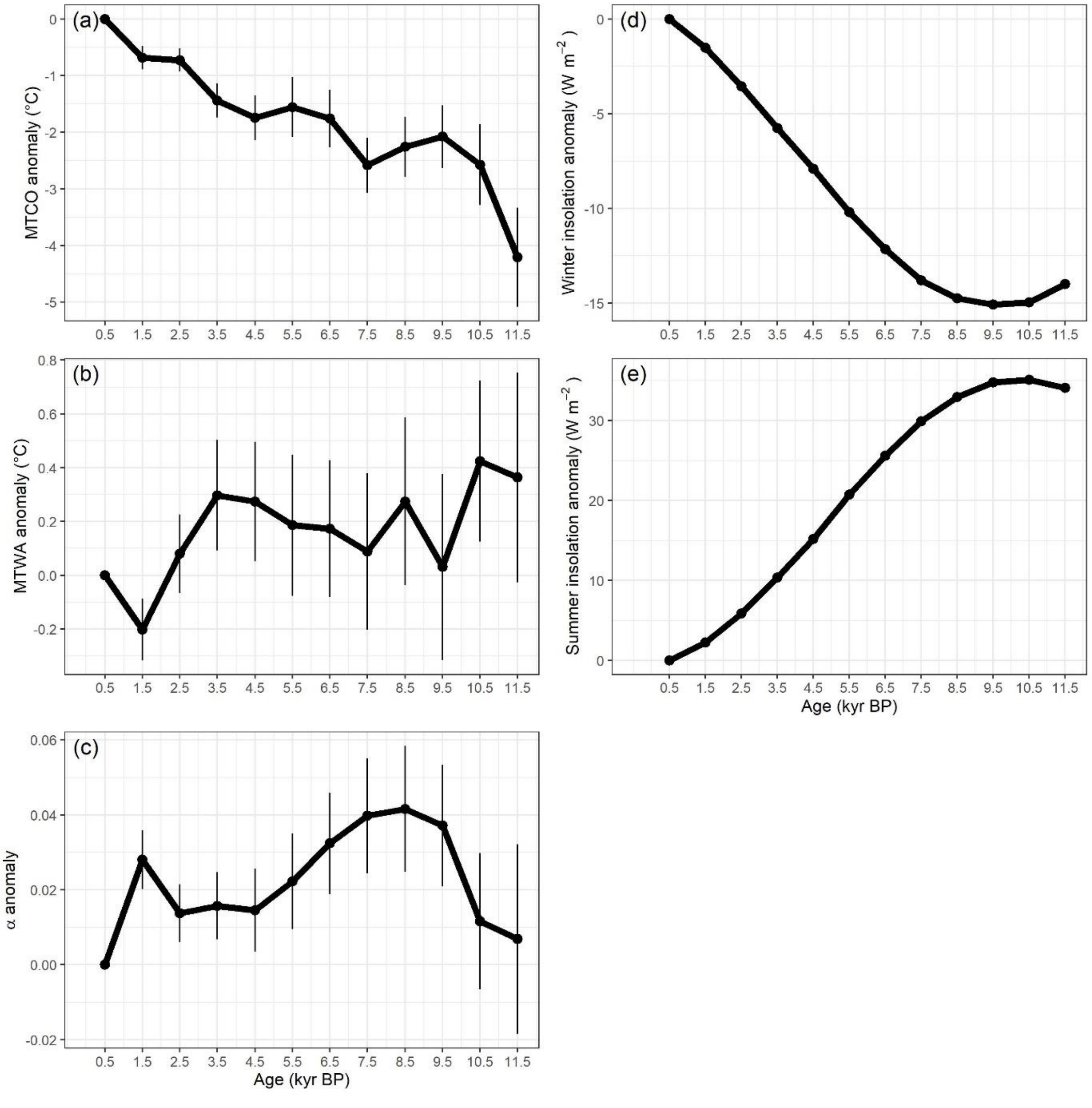

Figure 5. Changes in the west-east gradient of plant-available moisture as represented by anomalies in α relative to 0.5 ka at individual sites through the Holocene. The red lines show the regression lines. The shades indicate the 95 % confidence intervals of the regression lines.

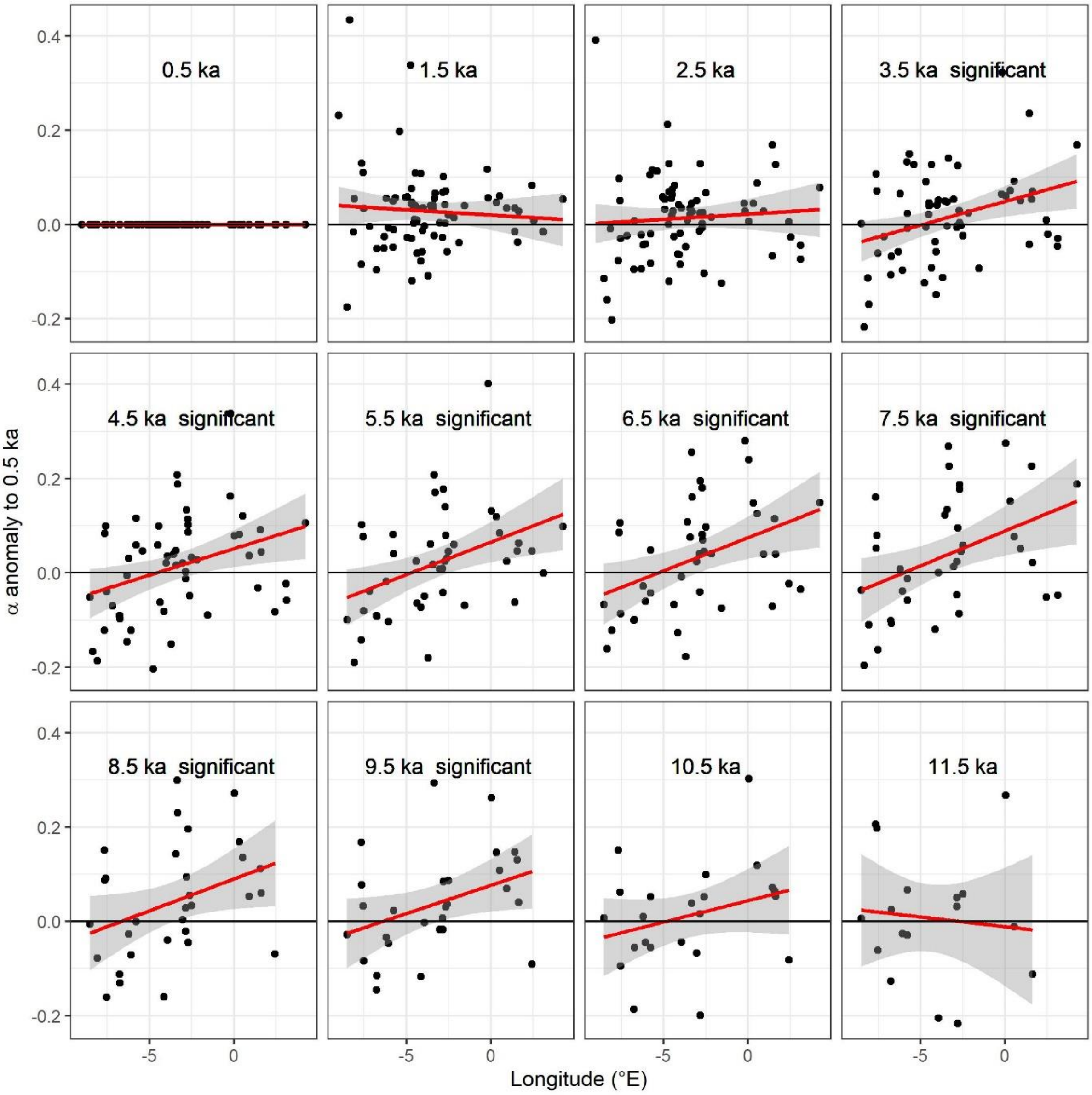

Figure 6. The relationship between mean temperature of the warmest month (MTWA) and plant-available moisture as represented by α (a) in the modern climate data set, and (b) in the Holocene reconstructions.

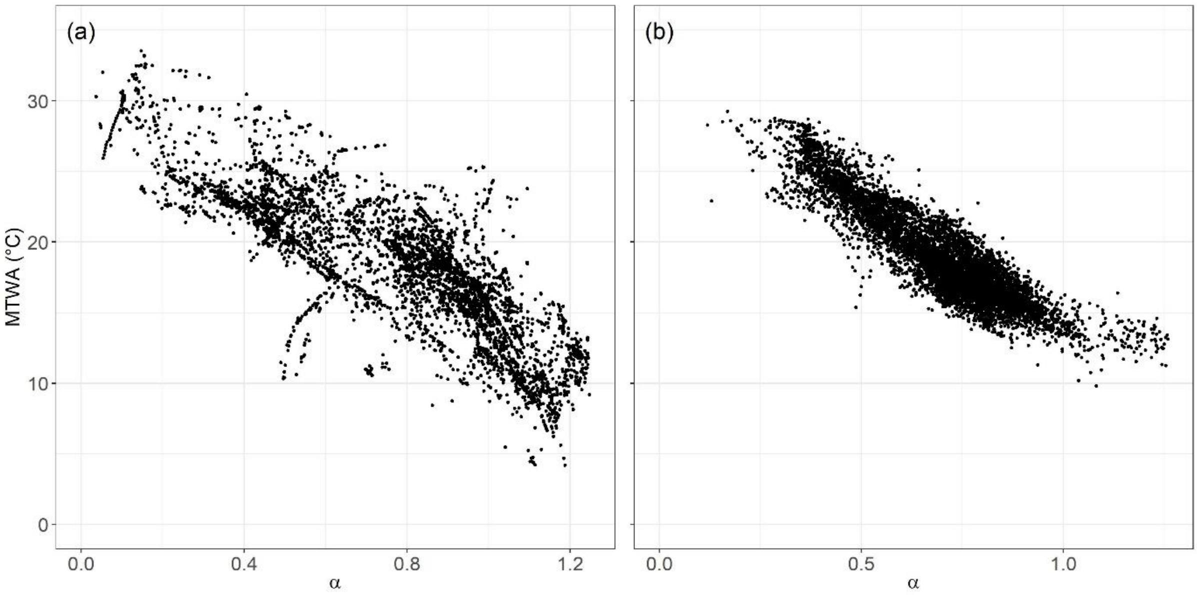

Table 1. Leave-out cross-validation (with geographically and climatically close sites removed) fitness of the modified version of fxTWA-PLS, for mean temperature of the coldest month (MTCO), mean temperature of the warmest month (MTWA) and plant-available moisture (α), with p-spline smoothed fx estimation, using bins of 0.02, 0.02 and 0.002, showing results for all the components. RMSEP is the root-mean-square error of prediction. ΔRMSEP is the per cent change of RMSEP using the current number of components than using one component less. *p* assesses whether using the current number of components is significantly different from using one component less, which is used to choose the last significant number of components (indicated in bold) to avoid over-fitting. The degree of overall compression is assessed by linear regression of the cross-validated reconstructions onto the climate variable, b_1, b_1.se are the slope and the standard error of the slope, respectively. The closer the slope (b_1) is to 1, the less the overall compression is.

	ncomp	R^2	avg. bias	max. bias	min. bias	RMSEP	ΔRMSEP	*p*	b_1	$b_1.se$
MTCO	1	0.70	−0.86	25.23	0.00	5.20	−39.97	0.001	0.89	0.01
	2	0.73	−0.73	25.00	0.00	4.87	−6.29	0.001	0.91	0.01
	3	0.74	−0.71	24.38	0.00	4.86	−0.32	0.001	0.91	0.01
	4	**0.75**	**−0.59**	**24.27**	**0.00**	**4.70**	**−3.26**	**0.001**	**0.91**	**0.01**
	5	0.74	−0.63	34.54	0.00	4.77	1.51	1.000	0.91	0.01
MTWA	1	0.52	−0.29	17.13	0.00	3.72	−26.88	0.001	0.69	0.01
	2	0.56	−0.14	17.20	0.00	3.53	−5.06	0.001	0.71	0.01
	3	0.56	−0.13	17.01	0.00	3.53	−0.20	0.008	0.71	0.01
	4	**0.57**	**−0.11**	**17.30**	**0.00**	**3.47**	**−1.56**	**0.001**	**0.71**	**0.01**
	5	0.57	−0.11	17.34	0.00	3.48	0.10	0.780	0.71	0.01
α	1	0.65	−0.014	0.787	0.000	0.165	−39.59	0.001	0.76	0.01
	2	0.68	−0.016	0.781	0.000	0.159	−3.55	0.001	0.77	0.01
	3	**0.68**	**−0.017**	**0.757**	**0.000**	**0.158**	**−0.61**	**0.023**	**0.78**	**0.01**
	4	0.69	−0.017	0.784	0.000	0.158	−0.43	0.108	0.79	0.01
	5	0.69	−0.017	0.850	0.000	0.158	0.26	0.985	0.80	0.01

Table 2. Canonical Correspondence Analysis (CCA) result of modern and fossil-reconstructed MTCO, MTWA and α. The summary statistics for the ANOVA-like permutation test (999 permutations) are also shown. VIF is the variance inflation factor, Df is the number of degrees of freedom, χ^2 is the constrained eigenvalue (or the sum of constrained eigenvalues for the whole model), F is significance, and Pr (>F) is the probability.

Modern	**Axes**	**Axis 1**	**Axis 2**	**Axis 3**	**VIF**
	Constrained eigenvalues	0.3819	0.1623	0.1087	/
	Correlations of the environmental variables with the axes:				
	MTCO	–0.815	0.579	0.012	1.31
	MTWA	–0.700	–0.203	0.685	3.34
	α	0.883	0.430	–0.187	3.39
		Df	χ^2	**F**	**Pr (>F)**
	Whole model	3	0.6530	78.113	0.001
	MTCO	1	0.3082	110.597	0.001
	MTWA	1	0.1602	57.489	0.001
	α	1	0.1846	66.252	0.001
	CCA 1	1	0.3819	137.076	0.001
	CCA 2	1	0.1623	58.252	0.001
	CCA 3	1	0.1087	39.011	0.001
Fossil-reconstructed	**Axes**	**Axis 1**	**Axis 2**	**Axis 3**	**VIF**
	Constrained eigenvalues	0.3601	0.2266	0.2037	/
	Correlations of the environmental variables with the axes:				
	MTCO	0.430	0.776	0.462	1.34
	MTWA	0.987	0.141	–0.076	5.40
	α	–0.947	0.088	–0.308	5.28
		Df	χ^2	**F**	**Pr (>F)**
	Whole model	3	0.7905	226.98	0.001
	MTCO	1	0.2465	212.34	0.001
	MTWA	1	0.3298	284.07	0.001
	α	1	0.2142	184.53	0.001
	CCA 1	1	0.3601	310.19	0.001
	CCA 2	1	0.2266	195.24	0.001
	CCA 3	1	0.2037	175.51	0.001

Table 3. Assessment of the significance of anomalies to 0.5 ka through time with latitude and elevation. The slope is obtained by linear regression of the anomaly onto the longitude or elevation. *p* is the significance of the slope (bold parts: $p < 0.05$). x_0 is the point where the anomaly is 0 in the linear equation, which indicates longitude or elevation where the anomaly changes sign.

		Longitude (°E)			Elevation (km)		
	age (ka)	slope	*p*	x_0	slope	*p*	x_0
MTCO (°C)	0.5	0.00	/	/	0.00	/	/
	1.5	−0.07	0.411	−13.02	−0.30	0.411	−1.21
	2.5	−0.15	0.095	−8.56	−0.52	0.179	−0.40
	3.5	−0.13	0.314	−14.83	−0.81	0.142	−0.77
	4.5	−0.12	0.444	−17.28	−0.69	0.319	−1.46
	5.5	−0.24	0.247	−9.49	−0.61	0.503	−1.43
	6.5	−0.18	0.372	−12.74	−0.87	0.293	−0.88
	7.5	−0.15	0.421	−20.39	−1.38	0.080	−0.67
	8.5	−0.03	0.890	−77.87	−1.58	0.065	−0.10
	9.5	0.01	0.954	156.31	−1.79	0.060	0.11
	10.5	0.20	0.474	9.25	−1.38	0.241	−0.64
	11.5	0.23	0.528	13.77	0.12	0.947	36.35
MTWA (°C)	0.5	0.00	/	/	0.00	/	/
	1.5	−0.01	0.862	−26.38	−0.05	0.830	−3.35
	2.5	−0.09	0.137	−2.80	−0.45	0.092	1.19
	3.5	**−0.23**	**0.005**	**−2.03**	−0.40	0.284	1.74
	4.5	**−0.21**	**0.016**	**−2.01**	−0.58	0.126	1.55
	5.5	**−0.26**	**0.011**	**−2.43**	−0.49	0.280	1.53
	6.5	**−0.24**	**0.017**	**−2.30**	−0.62	0.137	1.41
	7.5	**−0.26**	**0.012**	**−3.02**	**−1.05**	**0.019**	**1.28**
	8.5	−0.24	0.061	−2.43	**−1.15**	**0.023**	**1.57**
	9.5	**−0.32**	**0.013**	**−3.20**	−0.44	0.459	1.34
	10.5	−0.18	0.115	−1.23	0.54	0.276	0.44
	11.5	0.13	0.453	−7.25	0.37	0.663	0.22
α	0.5	0.00	/	/	0.00	/	/
	1.5	0.00	0.508	8.99	−0.01	0.393	3.40
	2.5	0.00	0.517	−9.89	0.02	0.249	0.19
	3.5	**0.01**	**0.006**	**−4.91**	0.02	0.191	0.28
	4.5	**0.01**	**0.010**	**−4.60**	**0.05**	**0.008**	**0.79**
	5.5	**0.01**	**0.005**	**−4.75**	**0.05**	**0.027**	**0.67**
	6.5	**0.01**	**0.007**	**−5.34**	**0.06**	**0.004**	**0.60**
	7.5	**0.02**	**0.009**	**−6.05**	**0.09**	**0.000**	**0.75**
	8.5	**0.01**	**0.049**	**−6.67**	**0.09**	**0.000**	**0.88**
	9.5	**0.01**	**0.048**	**−6.40**	**0.07**	**0.012**	**0.70**
	10.5	0.01	0.183	−4.85	0.02	0.535	0.59
	11.5	0.00	0.713	−2.76	0.03	0.654	0.93

Appendix A

Theoretical basis:

The previous version of fxTWA-PLS (fxTWA-PLS1):
The estimated optimum ($\hat{u}_k$) and unbiased tolerance ($\hat{t}_k$) of each taxon are calculated from the modern training data set as follows:

$$\hat{u}_k = \frac{\sum_{i=1}^{n} y_{ik} x_i}{\sum_{i=1}^{n} y_{ik}} \quad (A1)$$

$$\hat{t}_k = \sqrt{\frac{\sum_{i=1}^{n} y_{ik} (x_i - \hat{u}_k)^2}{(1 - 1/N_{2k})\ \sum_{i=1}^{n} y_{ik}}} \quad (A2)$$

where

$$N_{2k} = \frac{1}{\sum_{i=1}^{n} \left(\frac{y_{ik}}{\sum_{i'=1}^{n} y_{i'k}} \right)^2} \quad (A3)$$

where n is the total number of sites; y_{ik} is the observed abundance of the k^{th} taxon at the i^{th} site; x_i is the observed climate value at the i^{th} site; N_{2k} is the effective number of occurrences for the k^{th} taxon.

fx correction is applied as weight in the form of $1/fx^2$ at regression at step 7 in Table 1 in Liu et al. (2020). The regression step uses robust linear model fitting by the R code:

$$rlm\left(x_i \sim comp_1 + comp_2 + \cdots + comp_{pls}, weights = {}^{1}/_{fx^2}\right) \quad (A4)$$

The modified version of fxTWA-PLS (fxTWA-PLS2):
The distribution of y_{ik} is influenced by the distribution of the climate variable, so we need to apply the fx correction when calculating optimum and tolerance for each taxon as follows:

$$\hat{u}_k = \frac{\sum_{i=1}^{n} \frac{y_{ik} x_i}{f_{x_i}}}{\sum_{i=1}^{n} \frac{y_{ik}}{f_{x_i}}} \quad (A5)$$

$$\hat{t}_k = \sqrt{\frac{\sum_{i=1}^{n} \frac{y_{ik} (x_i - \hat{u}_k)^2}{f_{x_i}}}{\left(1 - \frac{1}{N_{2k}}\right) \sum_{i=1}^{n} \frac{y_{ik}}{f_{x_i}}}} \quad (A6)$$

where

$$N_{2k} = \frac{1}{\sum_{i=1}^{n} \left(\frac{\frac{y_{ik}}{f_{x_i}}}{\sum_{i'=1}^{n} \frac{y_{i'k}}{f_{x_{i'}}}} \right)^2} \quad (A7)$$

The modified version of fxTWA-PLS applies fx correction separately at taxon calculation and regression (step 2 and 7 in Table 1 in Liu et al., 2020), both using weight in the form of 1/fx. The regression step (step 7) then becomes:

$$rlm\left(x_i \sim comp_1 + comp_2 + \cdots + comp_{pls}, weights = {}^{1}/_{fx}\right) \qquad (A8)$$

The previous version uses fx values extracted from histograms, and different bin widths may result in different training results. The modified version applies P-splines histogram smoothing (Eilers and Marx, 2021) with third order difference penalty, which makes the fx values almost independent on the bin width. The optimal smoothing parameter of the P-spline penalty was determined by the HFS (Harville-Fellner-Schall) algorithm (Eilers and Marx, 2021) for the Poisson likelihood for the histogram counts.

Table A1. Leave-out cross-validation (with geographically and climatically close sites removed) fitness of the previous and modified version of fxTWA-PLS (fxTWA-PLS1 and fxTWA-PLS2, respectively), for mean temperature of the coldest month (MTCO), mean temperature of the warmest month (MTWA) and plant-available moisture (α), using bins of 0.02, 0.02 and 0.002, respectively. n is the number of components used. RMSEP is the root mean square error of prediction. ΔRMSEP is the per cent change of RMSEP using the current number of components than using one component less. *p* assesses whether using the current number of components is significantly different from using one component less, which is used to choose the last significant number of components (indicated in bold) to avoid overfitting. The degree of overall compression is assessed by doing linear regression to the cross-validation result and the climate variable. b1, b1.se are the slope and the standard error of the slope, respectively. The closer the slope (b1) is to 1, the lower the overall compression is. fx correction is set intrinsic in functions in `fxTWAPLS` package for both versions in this paper, instead of relying on an outside input in Liu et al. (2020), so the values of fxTWA-PLS1 might be slighted different from values in Table 2 in Liu et al. (2020), but it doesn't affect the conclusion.

	Method	n	R^2	avg. bias	max. bias	min. bias	RMSEP	ΔRMSEP	*p*	b1	b1.se
MTCO	fxTWA-PLS1	1	0.66	−0.86	31.17	0.00	5.21	−39.87	0.001	0.76	0.01
		2	0.72	−0.52	36.65	0.00	4.70	−9.78	0.001	0.80	0.01
		3	0.73	−0.47	41.18	0.00	4.62	−1.63	0.001	0.82	0.01
		4	**0.73**	**−0.51**	**44.86**	**0.00**	**4.58**	**−1.01**	**0.006**	**0.82**	**0.01**
		5	0.73	−0.41	58.35	0.00	4.62	0.89	0.708	0.83	0.01
	fxTWA-PLS2	1	0.70	−0.86	25.23	0.00	5.20	−39.97	0.001	0.89	0.01
		2	0.73	−0.73	25.00	0.00	4.87	−6.29	0.001	0.91	0.01
		3	0.74	−0.71	24.38	0.00	4.86	−0.32	0.001	0.91	0.01
		4	**0.75**	**−0.59**	**24.27**	**0.00**	**4.70**	**−3.26**	**0.001**	**0.91**	**0.01**
		5	0.74	−0.63	34.54	0.00	4.77	1.51	1.000	0.91	0.01
MTWA	fxTWA-PLS1	1	0.50	−0.53	17.91	0.00	3.87	−24.09	0.001	0.67	0.01
		2	**0.56**	**−0.54**	**17.71**	**0.00**	**3.52**	**−8.98**	**0.001**	**0.69**	**0.01**
		3	0.57	−0.49	25.14	0.00	3.52	0.09	0.565	0.73	0.01
		4	0.57	−0.43	34.92	0.00	3.56	1.12	0.974	0.75	0.01
		5	0.57	−0.46	32.23	0.00	3.55	−0.23	0.139	0.74	0.01
	fxTWA-PLS2	1	0.52	−0.29	17.13	0.00	3.72	−26.88	0.001	0.69	0.01
		2	0.56	−0.14	17.20	0.00	3.53	−5.06	0.001	0.71	0.01
		3	0.56	−0.13	17.01	0.00	3.53	−0.20	0.008	0.71	0.01
		4	**0.57**	**−0.11**	**17.30**	**0.00**	**3.47**	**−1.56**	**0.001**	**0.71**	**0.01**
		5	0.57	−0.11	17.34	0.00	3.48	0.10	0.780	0.71	0.01
α	fxTWA-PLS1	1	0.63	−0.020	0.773	0.000	0.174	−36.23	0.001	0.78	0.01
		2	0.69	−0.012	0.902	0.000	0.157	−9.66	0.001	0.79	0.01
		3	**0.69**	**−0.011**	**0.820**	**0.000**	**0.155**	**−1.28**	**0.001**	**0.79**	**0.01**
		4	0.70	−0.010	0.786	0.000	0.156	0.25	0.867	0.81	0.01
		5	0.70	−0.010	0.786	0.000	0.156	0.09	1.000	0.81	0.01
	fxTWA-PLS2	1	0.65	−0.014	0.787	0.000	0.165	−39.59	0.001	0.76	0.01
		2	0.68	−0.016	0.781	0.000	0.159	−3.55	0.001	0.77	0.01
		3	**0.68**	**−0.017**	**0.757**	**0.000**	**0.158**	**−0.61**	**0.023**	**0.78**	**0.01**
		4	0.69	−0.017	0.784	0.000	0.158	−0.43	0.108	0.79	0.01
		5	0.69	−0.017	0.850	0.000	0.158	0.26	0.985	0.80	0.01

Figure A1. Training results using the last significant number of components. The left panel shows the previous version (fxTWA-PLS1) and the right panel shows the modified version of fxTWA-PLS (fxTWA-PLS2). The 1: 1 line is shown in black; the linear regression line is shown in red, to show the degree of overall compression. The horizontal dashed lines indicate the natural limit of α (0~1.26).

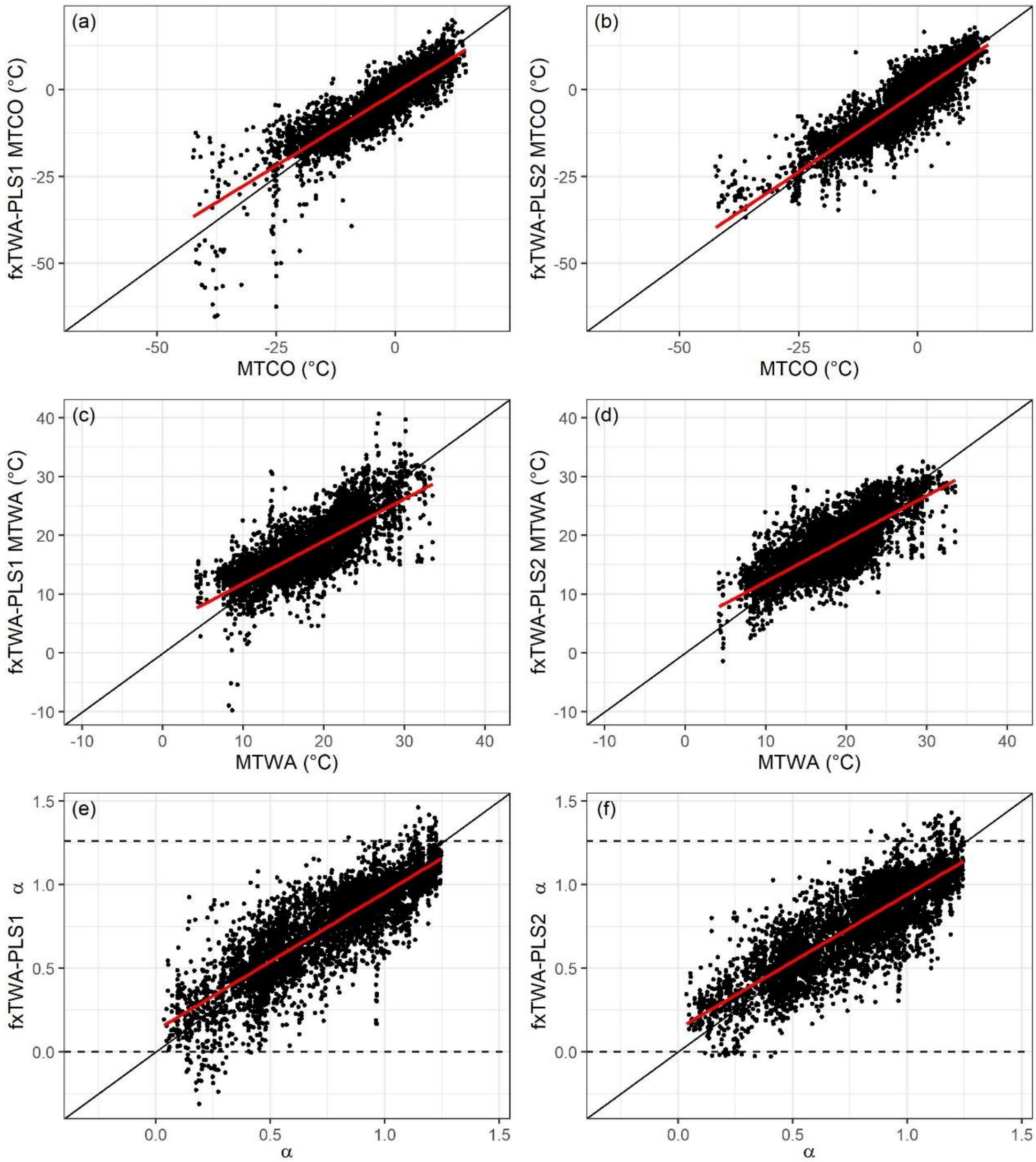

Figure A2. Residuals using the last significant number of components. The left panel shows the previous version (fxTWA-PLS1) and the right panel shows the modified version (fxTWA-PLS2) of fxTWA-PLS. The zero line is shown in black; the locally estimated scatterplot smoothing is shown in red, to show the degree of local compression.

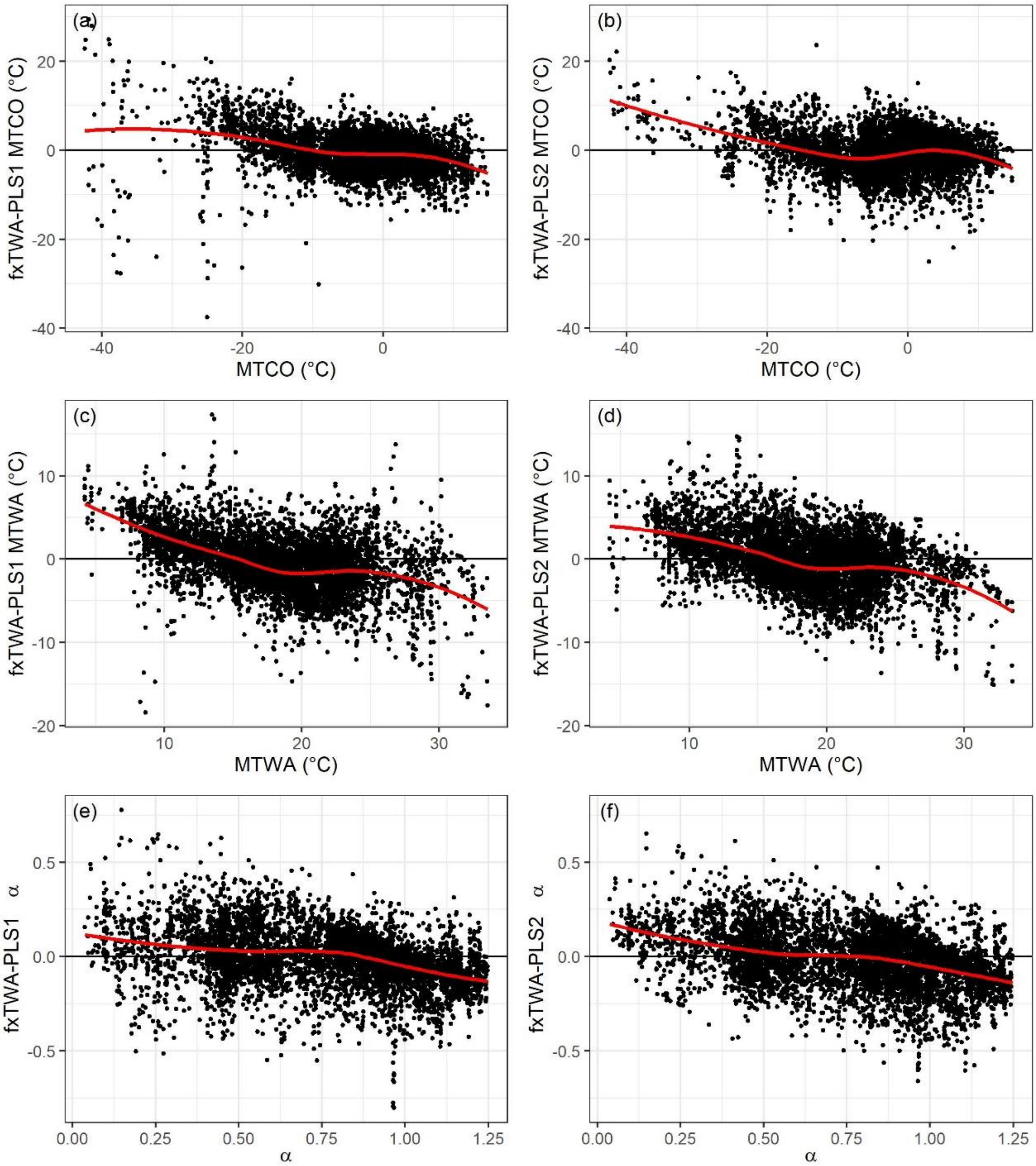

As shown in Table A1, Figure A1 and A2, the modified version is able to further reduce the compression in MTCO and MTWA, and maximum bias in MTCO, MTWA and α. As shown in Figure A1 and A2, there is less scatter and there are less α values beyond the natural limit.